

**Provisional Annual Statement on the Status of Global Climate in 2015**

**Contents**

2015 likely to be the warmest year on record.....	2
A Strong El Niño in 2015.....	2
Impacts of El Niño .....	3
Ocean heat and sea level rise.....	4
Regional temperatures .....	4
Heatwaves.....	5
Rainfall and drought.....	6
Africa .....	6
Asia.....	7
South America .....	7
North America.....	8
South-West Pacific.....	8
Europe.....	8
Wildfires .....	9
Tropical storms .....	9
Snow and Ice .....	10
Greenhouse Gases and Radiative Forcing .....	11
Stratospheric Ozone and Ozone-depleting Gases .....	12
Tables .....	13
Figures .....	14

## 2015 likely to be the warmest year on record

The long-term rise in global temperatures, the dominant cause of which is the anthropogenic emission of greenhouse gases, combined with the effects of a developing El Niño, have resulted in unusual global warmth in 2015.

The global-average near-surface temperature for 2015 is likely to be the warmest on record according to data sources<sup>1</sup> analysed by the WMO (**Figure 1, Figure 14**). A preliminary estimate based on data from January to October shows that the global average temperature for the year so far was around  $0.73 \pm 0.09^\circ\text{C}$  above the 1961-1990 average of  $14.0^\circ\text{C}$  and approximately  $1^\circ\text{C}$  above the 1850-1899 period, although uncertainties relative to this earlier period are larger and more difficult to estimate.

These estimates are based on air temperature data gathered at meteorological stations over land and on sea-surface temperatures measured at sea by ships in the voluntary observing fleet and by drifting and moored buoys.

Global-average temperatures can also be estimated using output from reanalyses. Reanalyses provide a consistent synthesis of many data streams using a modern weather forecasting system. Two long-term reanalyses were surveyed: the ERA-Interim reanalysis, produced by the European Centre for Medium-Range Weather Forecasts and the JRA-55 reanalysis produced by the Japan Meteorological Agency. The central estimates for both these reanalyses for the period January to October, indicate that 2015 is currently the warmest year on record.

An anomaly of  $0.73^\circ\text{C}$  for the year would place 2015 as nominally the warmest year on record. The central estimates of each of the data sets and reanalyses considered by the WMO individually would place 2015 as the warmest year with the difference between 2015 and the next warmest year currently lying between  $0.04$  and  $0.15^\circ\text{C}$  (**Table 1**).

The global average land temperatures averaged over January to October suggest that 2015 is also set to be the joint warmest year on record over land (2007 and 2010 are comparable). The global average sea-surface temperature, which set a record last year, is likely to equal or surpass that record in 2015.

## A Strong El Niño in 2015

Variations in the temperature of the surface waters of the tropical Pacific combine with atmospheric feedbacks to drive the two distinct phases of the El Niño Southern Oscillation (ENSO): El Niño and La Niña. During an El Niño, sea-surface temperatures in the eastern tropical Pacific rise above average. This leads to a weakening, or reversal, of the prevailing trade winds, which acts to reinforce the surface warming. ENSO is the leading mode of year-to-year climate variability. El Niño affects the global atmospheric circulation, altering weather patterns around the world and temporarily elevates global temperatures.

In 2015, sea-surface temperatures in the central Pacific increased, exceeding typical El Niño thresholds around May (**Figure 4**). Atmospheric indicators such as the pressure difference

---

<sup>1</sup> HadCRUT4.4.0.0 produced by the Met Office Hadley Centre and the Climatic Research Unit at the University of East Anglia; GISTEMP produced by the National Aeronautical and Space Administration Goddard Institute of Space Studies; and NOAA GlobalTemp produced by the National Oceanic and Atmospheric Administration National Centres for Environmental Information. The quoted number is an average of these three data sets.

between Tahiti and Darwin, enhanced convection near the dateline, and weakening of the trade winds, were also indicative of a developing El Niño. El Niño continued to strengthen through late October and early November. At the start of November, sea-surface temperatures were comparable to those recorded during the exceptionally strong El Niño events in 1997/1998 and 1982/1983.

### Impacts of El Niño

El Niño affects rainfall and weather patterns in many places around the world. Although the precise details of any single El Niño will differ from one to the next, there are certain recurrent patterns that might be expected during a strong El Niño.

El Niño is typically associated with higher global temperatures both at the surface and through the troposphere. However, there is a lag between warming of the tropical Pacific and its effect on global temperatures. The lag is longer in the troposphere than at the surface. Although global surface temperatures might have been slightly elevated by the near-El Niño conditions that prevailed in late 2014, the full effect of the strong 2015 El Niño on global temperature is likely to continue after El Niño peaks.

During El Niño, rainfall deficits are usually experienced from Central America down through to Brazil. Puerto Rico (**Figure 3**), has seen rainfall totals below the long-term average, leading to drought and water rationing in some areas. Large areas of Central America and the Caribbean recorded below average rainfall for the year so far. Brazil, which started the year in drought in southern and eastern areas, saw the focus of the drought shift north with scant rainfall during the dry season over the Amazon. There is also a connection with reduced Monsoon rainfall over India. In 2015, monsoon rainfall over India was 86% of normal.

At the other side of the Pacific, El Niño is usually associated with reduced rainfall across the Pacific islands and Indonesia. Global and local analyses (**Figure 3, Figure 5**) of precipitation show severe rainfall deficits across the region. In Indonesia, the low rainfall has likely increased the risk and incidence of wildfires, which have led to poor air quality. In the first half of the year, 40 provinces in upper Thailand experienced the second lowest total rainfall in 64 years. Eastern Australia typically sees reduced rainfall during El Niño. After a very wet January, the period from February to October in the Northern Territory, Queensland and Victoria saw rainfall totals that were very much below average although not as consistently as one might expect from a strong El Niño.

While, El Niño typically brings drought to some areas, it brings above average rains to others. Areas of Peru typically see increased rainfall and, in 2015, Peru was affected by heavy rain and flooding. In August, heavy rain in the Buenos Aires province of Argentina triggered flooding along the “El Salado” basin.

Moreover, El Niño affects tropical cyclone formation and development, reducing the formation of hurricanes in the North Atlantic and promoting the formation of hurricanes and typhoons in the Pacific, consistent with what has been seen this year (see the section on **Tropical storms**).

The warming waters associated with El Niño have a direct effect on marine ecosystems. For instance, when temperatures are too high, coral reefs “bleach”, expelling the symbiotic algae that are their main source of food. In early October, NOAA declared that record global ocean

temperatures had led to a global bleaching event, with bleaching events observed in all three ocean basins. The bleaching began in the North Pacific in the summer of 2014 and spread to the South Pacific and Indian Ocean in 2015.

Variability of the climate in the Pacific also plays a role over longer periods. The Pacific Decadal Oscillation (PDO), which has been in a predominantly negative phase since 2000, has been implicated in the reduced rate of global warming since the turn of the century. In 2014 and 2015, the PDO was strongly positive; however, because both the ENSO and PDO have similar patterns, it is too early to say whether this reflects a longer term return to positive conditions.

### **Ocean heat and sea level rise**

The oceans have absorbed around 90% of the energy that has accumulated in the climate system. The IPCC 5<sup>th</sup> Assessment Report concluded that “it is very likely that anthropogenic forcings have made a substantial contribution to increases in global upper ocean heat content (0-700m) observed since the 1970s”. This energy is associated with an increase in the temperature and hence in the volume of the oceans. The increased volume, together with effects from the melting of ice from glaciers and ice sheets, and changing land storage, has led to an overall increase in global-average sea level.

In the first eight months of 2015, global ocean heat content through both the upper 700m and 2000m of the oceans reached record levels (Figure 6). Routine measurements of temperatures down to 2000m are now made using Argo floats and near-global coverage of Argo measurements has been achieved since the mid-2000s. Since then there has been a clear increase in ocean heat content down to 2000m.

Sea level is measured by satellites (Figure 7) as well as by traditional tide gauges. The latest estimates of global sea level from satellite altimeters indicate that the global average sea level in the first half of 2015 was the highest in the satellite record and, given, the long-term upward trend in sea level as estimated from tide gauges, the highest in more than a century.

Even though the global average sea-level was at or near record levels in 2015, not all areas were. Recently<sup>2</sup>, monthly average sea levels were lower than normal in the western tropical Pacific, as might be expected during El Niño. Tide gauges in the Marshall Islands and Federated States, Papua New Guinea, Solomon Islands, Vanuatu and Tonga have showed below average sea levels.

### **Regional temperatures**

For the period January to October 2015, significant warmth was recorded over the majority of observed land areas (Figure 2). Particularly warm were western areas of North America, where eight US States had their warmest January to October on record, large areas of South America, Africa and southern and eastern Eurasia. Russia had its warmest January to September and China had its warmest January-to-October period on record. For the continent of Africa, 2015 currently ranks as the second warmest year on record. Western Canada was unusually warm with record winter average temperatures reported along the Pacific coast. The Hong Kong observatory reported its warmest summer. Australia had its

---

<sup>2</sup> <http://www.bom.gov.au/ntc/IDO60101/IDO60101.201510.pdf>

warmest October on record and a heatwave early in the month set new records for early season warmth in Southern Australia. The Faroe Islands had their warmest October since 1920 and the third warmest since 1890.

Few areas experienced significant cold conditions averaged over the year. One notably cold area was the Antarctic, where the positive phase of the Southern Annular Mode persisted for several months. October saw a change to more neutral conditions and a warming over the continent. Eastern areas of north America were colder than average during the year. None were record cold for the year, but February was the 2<sup>nd</sup> coldest on record for some states. After a warm January to September, Argentina experienced its coldest October on record.

Over the oceans, significant warmth was recorded across large areas. The Tropical Pacific was much warmer than average, exceeding 1°C over much of the central and eastern equatorial Pacific, as would be expected during El Niño. The northeast Pacific, much of the Indian Ocean and areas in the north and south Atlantic were significantly warm too. SSTs in the Indian Ocean reflect the positive phase of the Indian Ocean Dipole, which affects the climate locally. Areas to the south of Greenland and in the far southwest Atlantic were significantly colder than average. Other areas of the Southern Ocean (roughly, south of 60°S) were colder than average, but in many cases there are too few data to reliably estimate the significance of current anomalies.

### Heatwaves

A major heat wave affected India from around 21 May to the 10 June. In the last ten days of May, average maximum temperatures exceeded 42°C widely and 45°C in some areas (Figure 8). Average temperatures exceeding 45 °C were recorded with some locations reaching 48.0°C e.g. Khammam on 24 May 2015 and Churu on 19 June. Over 2000 people are reported to have died due to the heat. A period of extreme temperatures also affected southern Pakistan from 17<sup>th</sup> June to 24<sup>th</sup> June, where temperatures exceeded 40 °C. More than 1400 died in the heat in Karachi and around 200 in other parts of Sindh province. Whilst extreme heat is common in the pre-monsoon season in the Indian subcontinent, in 2015 the heat extended over a larger area than normal, incorporating regions such as Andhra Pradesh in eastern India and coastal Pakistan, and was also accompanied by very high humidity in places.

Heat waves affected Europe, northern Africa and the Middle East through the late spring and summer with the focus of the heat shifting from month to month.

In May, high temperatures affected Burkina Faso, Niger and Morocco. In Morocco new temperature records for the month were set at some stations. Niger saw a run of days when temperatures exceeded 41°C. Spain and Portugal also saw unusually high temperatures, with 42.6°C recorded at Lanzarote airport and Valencia airport, both readings exceeding the previous highest May temperatures by 6°C. In Portugal, Beja had 19 days when the maximum temperature exceeded 30°C; the May average is 5 days. In June, high temperatures affected Niger, with 46.7°C registered at Bilma.

July brought heat waves to a large area from Denmark in the north, to Morocco in the south and Iran in the east. Denmark experienced regional heat waves at the start of July with temperatures above 30°C. In the UK, Heathrow recorded the highest July temperature on record for the UK with 36.7°C on 1<sup>st</sup> July. In France and Spain, a number of stations broke

records for their highest temperatures, including 41.1°C at Saint-Etienne on the 7<sup>th</sup>, and 44.9°C at Zaragoza airport. Germany recorded a new country-wide record with 40.3°C at Kitzingen on the 5<sup>th</sup> and Geneva in Switzerland reported 39.7°C on the 7<sup>th</sup>, a new record. High temperatures were accompanied by low rainfall totals with parts of France experiencing record low monthly precipitation. Spain had its warmest July on record and a heatwave from 27 June to 22 July was by far the longest recorded in Spain. Ljubljana in Slovenia reported a record 21 days when the maximum temperature exceeded 30°C. Austria reported its warmest July since at least 1767. Extreme heat in July in Morocco led to nearly 50% loss of citrus fruit production. In Egypt, maximum temperatures for the month reached 47.6°C at Luxor. On 31<sup>st</sup> July, Bandar Mahshahr, a coastal city in Iran, recorded a temperature of 46°C combined with a dew point temperature of 32°C. The high temperature combined with high humidity is exceptional.

From 1 to 4 August, Jordan experienced a heatwave, with temperatures reaching 47.0°C at Wadi Elrayyan station on the 2<sup>nd</sup>, nearly 8°C above normal. Wroclaw (Poland) experienced an all-time high temperature of 38.9°C on the 8<sup>th</sup> August. The heat continued into September, shifting further into Eastern Europe.

During the spring of 2015 in South Africa, record high temperatures were exceeded on a regular basis. On 27 October, Vredendal recorded 48.4°C. Early November saw a continuation of the heatwave with 40.3°C recorded at Pretoria and 36.5°C in Johannesburg both all-time records for those stations.

### **Rainfall and drought**

Figure 3 shows percentiles for January to October precipitation in 2015. Areas of high rainfall included: southern areas of the US, Mexico, Bolivia, southern Brazil, southeast Europe, areas of Pakistan and Afghanistan. Dry areas included Central America and the Caribbean, northeast South America including Brazil (reflecting the ongoing drought in the region), parts of central Europe, parts of Southeast Asia, Indonesia and southern Africa. Although long term accumulations are important, they can disguise great variability in short term totals. For example, in Niger, despite an average for the year so far that was close to the long-term mean, heavy rain exceeding 100mm in a day, was recorded at a number of locations leading to floods that killed 25.

### **Africa**

Heavy rain in January in south east Africa led to flooding in Malawi and Zimbabwe. In Mozambique, which was also affected, the flooding also exacerbated an outbreak of Cholera. In February, heavy rain affected Morocco, Algeria and Tunisia. At Alhoceima in Morocco, where the normal monthly rainfall is 35.9mm, February 2015 saw 206.1mm, of which 88.4 mm fell in 24 hours on February 18.

In Tanzania, heavy rain and floods affected the country in March, May and November. On 3<sup>rd</sup> March, heavy rainfall accompanied by hail and high winds hit Mwakata Ward in Tanzania killing 50 people. In the south-western highlands on 4<sup>th</sup> November, 327.8mm of rain was recorded at the Tukuyu station, the highest recorded at the station. Heavy rain at Mwanza on 1<sup>st</sup> November caused severe flooding, killing six. Heavy rain in early May led to further flooding.



Mauritius, in the southwest Indian Ocean, had its wettest June since 1976. Total rainfall for the month was 180% of the long term average. Heavy rainfall during the night of the 23 June caused a major landslide.

In South Africa, the season from July 2014 to June 2015 was, on average, the driest season since the 1991/1992 season and the third driest in a series which begins in the 1932/1933 season. By the end of summer, the prolonged drought conditions severely affected the maize, sugar cane and sorghum harvests. The dry conditions are ongoing with no significant rain having yet been received in the early part of the 2015-2016 rainy season.

In Burkina Faso there was significant flooding with strong winds in some areas in July and August which affected over 20,000 people. 2015 saw exceptional seasonal rainfall totals, exceeding 1000mm in several parts of the country. Heavy rains also affected Mali. In Morocco on 6<sup>th</sup> August, Marrakech received 35.9mm of rain in one hour, which is over 13 times the monthly normal of 2.7mm.

On 24 September, unusually heavy rain affected the western coastal region of Libya with 100mm falling in 24 hours, triggering flash floods.

## Asia

The Indian monsoon onset at Kerala was on 5<sup>th</sup> June, four days later than average. Rainfall, recorded between June and September, was 86% of its long term average. 2014 also saw below average rainfall, the fourth time in the 115-year record that two consecutive years have been below average. Monsoon season fatalities by floods and landslides were reported as exceeding 660 in India.

In Pakistan, the summer monsoon was erratic, and 90% of the seasonal total was concentrated over the first half of season in areas which the rain seldom reaches. One station recorded 540mm of rain in 24 hours; the annual normal is 336mm. Pakistan also saw unseasonal weather totals during March and April, which heavy rain and late frost causing damage to crops. A rare tornado hit the Peshawar valley on 27<sup>th</sup> April, killing 45 people.

Between May and October, China experienced 35 heavy rain events. Subsequent flooding affected 75 million people with estimated economic losses of 25 billion dollars. Between 5<sup>th</sup> and 31<sup>st</sup> May, the Huanan region in the northeast of the country received rainfall totalling over 150% of the long term average, slightly more than 2014 and the most in nearly 40 years.

Drought over Russia during the late spring and summer led to crop failures over more than 1.5 million hectares with associated economic losses totalling around 9 billion roubles. The following were particularly affected: the Volgograd and Saratov regions along the Volga River, as well as Orenburg to the east, but also the southwestern part of European Russia, the Republic of Kalmykia, as well as the south central part of Siberia, the Republic of Buryatia; the latter region experienced forest fires that burnt 700,000 hectares.

## South America

During January, Chile was drier than average throughout the country with the south of the country seeing the most extreme deficits. In places it was the driest January in at least 50 years. The stations at Temuco and Valdivia, situated halfway down the country, recorded no rainfall during the month, Osorno and Puerto Montt recorded 1.8 mm and 9.6 mm

respectively. In February, heavy rain in Argentina saw a number of long-running stations break their February precipitation records. The Córdoba Observatory recorded 385.4 mm of rain for the month, beating the long-standing record of 266.4mm set in 1889. March in Chile saw unusually heavy rains in the southern Atacama which caused flooding and mudslides in contrast to dry conditions further south. In August, heavy rain in the Buenos Aires province of Argentina saw several monthly and daily rainfall records broken during the month. The rain triggered flooding along the “El Salado” basin which affected thousands of people.

Other high impact rainfall and drought events for this region – such as the drought in Brazil – are covered in section on the **Impacts of El Niño**.

### North America

It was the wettest May on record for the contiguous US and the wettest month overall in 121 years of record keeping. Colorado, Oklahoma, and Texas were each record wet for the month. The May rains effectively ended the drought that had affected the Southern Plains since 2011. Further west, however, long-term drought conditions continued. Basins across the west depend on snowpack as a water resource. On April 1, the snow water equivalent was 5% of normal in the west which is the lowest since measurements began in 1950. The previous lowest was 25% of normal, recorded in 1977 and 2014.

In early October, as hurricane Joaquin moved off the east coast, it interacted with a low pressure system to pull tropical air into the Carolinas. Record rainfall totals of 380-500mm were widespread with significant flooding across the region, which killed sixteen. Extreme rainfall and flash flooding, some of it associated with remnants of hurricane Patricia, also affected parts of Texas.

Mexico had its wettest March on record (since 1941). The rainfall nationally was 69.6mm, 54.9mm above the long-term average of 14.7mm. In the northwest of Mexico, in June, Baja California and Baja California Sur had their wettest June on record (since 1941). Sonora had its second wettest June. In the centre and north of the country, Aguascalientes and Zacatecas, were third wettest.

Low rainfall totals for the year were widespread through Central America and the Caribbean, see the section on **Impacts of El Niño**.

### South-West Pacific

For specific extreme rainfall and drought events in this region see Section on **Impacts of El Niño and Tropical storms**.

### Europe

January was wet through large areas of northern Europe and Scandinavia. In western parts of Finland many weather stations reported record high precipitation totals for the month. In Sweden, Piteå reported a new record of 134.6 mm for January, the wettest since at least 1860. Several other station records were broken in Sweden.

In February, heavy rain affected countries in southern Europe including Italy and the southern Balkan Peninsula. There was flooding in southern and south-eastern parts of Albania, the former Yugoslav Republic of Macedonia, Greece and Bulgaria.



In May, Sweden was very wet across almost the entire country. Several stations with rainfall records exceeding 100 years hit their monthly records. In Stockholm, it was the wettest May in 200 years. Norway had its second wettest May on record.

France saw three periods marked by particularly heavy rainfall. The first on 23-24 August, saw Montpellier in the Languedoc region receive 154mm of rain in 3 hours, with 108.1mm falling in one hour, the highest 1 hour total recorded at the site. Other stations recorded in excess of 200mm of rain over the two days. From 12-13 September, a number of stations recorded rainfall totals in excess of 200mm. On the 12<sup>th</sup> 112.2mm fell in one hour at La Vacquerie and 119.7mm fell in one hour at Soumont in the South of France. During the third period on 3 October, storms brought heavy rain to the southeast of France. Close to 200mm of rain fell in 2 hours in parts of the Alpes-Maritimes region and 20 people were killed. In Spain, between 20 and 24 March, 300mm of rain fell in some areas of Castellon province.

### Wildfires

The dry and warm conditions observed across much of the western U.S. during the year favoured the development of wildfires. In Alaska, over 400 fires burned 728,000 hectares in May, breaking the previous record of 216 fires and 445,000 hectares. Over 700 wildfires were reported in Alaska during July, burning nearly 2 million hectares during the summer. Large fires burned throughout the Northwest in August. Lightning on August 14 ignited the Okanogan Complex Fire and it grew to be Washington's largest fire on record at over 121,000 hectares. The Soda Fire in southwest Idaho began August 10 and consumed over 113,000 hectares, displaced wildlife, and damaged locations of historic significance. The Rocky Fire in Lake County, northern California began on July 29 and spread rapidly with high winds during the first few days of August. The Rocky fire burned over 28,000 hectares and destroyed 43 residences. The Rough Fire in southern Sierra Nevada was ignited by lightning on 31<sup>st</sup> July and grew to over 31,000 hectares by the end of August.

### Tropical storms

Globally, a total of 84 named tropical storms formed between the start of the year and 10 November. A named storm is defined as a tropical storm where the maximum sustained surface wind speed equals or exceeds 63 km hr<sup>-1</sup>. This is equal to the 1981-2010 annual average of around 85 storms, but the year is not yet over. The lowest number of storms in a year in the modern satellite era was 67 storms in 2010.

In the **North Atlantic** basin, there were 12 named storms of which 4 became hurricanes and 2 of these (Danny and Joaquin) were classified as major hurricanes. This is slightly below the long-term average of 12.1 storm, 6.4 hurricanes and 2.7 major hurricanes. Hurricane activity in the North Atlantic is typically suppressed during an El Niño. Accumulated Cyclone Energy (ACE), is a measure of the combined strength and duration of tropical storms. In 2015, the ACE for the Atlantic basin to the end of October was about 58% of the long-term average.

In the **Northeast Pacific** basin (up to November 10), 17 named storms formed. 12 of these storms became hurricanes and 9 developed further to become major hurricanes. The averages for a year are 16.5 storms, 8.9 hurricanes and 4.3 major hurricanes respectively. Patricia was the strongest hurricane on record in either the Atlantic or eastern North Pacific

basins, with maximum sustained wind speeds of 200 mph. It made landfall on the Mexican coast on 24 October in a sparsely populated area and there were no reported casualties. The remnants of Patricia contributed to heavy rainfall and flooding in the Southern Plains and lower Mississippi River Valley. The ACE for the north east Pacific through the end of October was about 50 percent higher than the long term average. The **Central Pacific** region experienced six named storms in total, three of which reached hurricane strength.

In the **Northwest Pacific** basin, 25 named storms were recorded (to the end of October). Of these, 16 reached typhoon strength. The averages for a whole year are 25.7 storms (22.1 to the end of October) and 16.6 typhoons. Typhoon Koppu, known locally as Lando, made landfall in the Philippines in October affecting many people and causing widespread damage. Because of the tracks taken by the storms, for the first time since 1946 no storm warnings had to be issued in Hong Kong in August or September. Six typhoons made landfall over China, with three – Chan-hom, Soudelor and Mujigae – leading to combined estimated economic losses of 8 billion dollars.

Four named storms formed in the **Northern Indian Ocean**, compared to an average of 4.9 for a year. Komen developed as a tropical depression over the Ganges delta. It strengthened at sea before making landfall as a tropical storm. Rainfall associated with the storm and monsoon rains led to severe flooding and landslides in Myanmar. Bangladesh also suffered from flash floods and landslides. The storm came after an earlier period of heavy rains from the 24 June. Tropical cyclone Chapala made landfall in Yemen, leading to substantial flooding. This was the first tropical cyclone to make landfall in Yemen at (cat. 1) hurricane strength. Socotra Island was affected by both Chapala and cyclone Megh which developed shortly after Chapala made landfall. Both were category 3 storms when they passed the island.

In the **South West Indian Ocean**, 8 named storms developed with a 9<sup>th</sup> storm (Ikola) crossing over from the Australian basin bringing the total up to the long-term average.

In the **Australian** basin, there were 7 named storms, slightly below the long-term average of 10. Cyclone Marcia was the most intense landfall known so far south on the east coast, at least in the modern satellite era. The timing of Raquel - at the end of June - was unusual. Such a late storm was not recorded in the eastern Australian region in the satellite era and the only previous winter cyclone recorded was in early June 1972.

The **South Pacific** saw 9 named storms (4 of which overlapped with the Australian basin). The average for a year is 6.3. Tropical cyclone Pam made landfall over Vanuatu as a category 5 cyclone on 13 March destroying many homes. The government of Tuvalu declared a State of Emergency on 13 March following severe inundations from storm surge and sea swell. Kiribati reported severe damage in its three southern islands. The Solomon Islands were also affected.

## Snow and Ice

In the northern hemisphere, the seasonal cycle of Arctic sea-ice extent usually peaks in March and reaches a minimum in September. Since consistent satellite records began in the late 1970s, there has been a general decline in sea ice extent throughout the seasonal cycle (**Figure 10**). In 2015, the daily maximum extent, which occurred on 25<sup>th</sup> February, was the lowest on record at 14.54 million km<sup>2</sup>, 1.10 million km<sup>2</sup> below the 1981-2010 average and

0.13 million km<sup>2</sup> below the previous record set in 2011. The minimum sea ice extent was on 11<sup>th</sup> September when the extent was 4.41 million km<sup>2</sup>. This was the fourth lowest minimum extent in the satellite record.

In the southern hemisphere, the seasonal cycle of Antarctic sea-ice extent typically peaks around September or October and reaches a minimum in February or March (**Figure 11**). In 2015, the daily maximum extent of 18.83 million km<sup>2</sup> was recorded on 6<sup>th</sup> October. This is the 16<sup>th</sup> highest maximum extent in the satellite record. The minimum extent, recorded on 20 February, was 3.58 million km<sup>2</sup>, the fourth highest summer minimum extent on record. The year-to-year variability of the Antarctic sea ice minimum extent is large compared to the long term trend; the past five years have seen the second highest recorded monthly extent (2013) and the third lowest (2011).

In Greenland, the total summer melt extent area in 2015 was the 11<sup>th</sup> largest on record (since 1978). This is above the long-term average, but not unusual in the context of the past decade. At the Greenland summit station run by DMI, winter, spring and summer temperature were below average. A new record August low temperature of -39.6°C was recorded on 28<sup>th</sup> August. In October, the lowest recorded temperature of -55.2°C on the 24<sup>th</sup> of the month equalled the record low reported on 31<sup>st</sup> October 2007.

The snow extent in the northern hemisphere during spring was 28.5 million km<sup>2</sup> which is below the long term average and the 8<sup>th</sup> lowest on record. North America had its 4<sup>th</sup> lowest spring snow extent on record.

In the US, numerous snow storms affected the northeast during February. Boston and Worcester (Massachusetts) had their all-time snowiest month and snowiest winter. Boston received 164.6 cm of snow during February, which is more than the city normally gets in an entire season.

### Greenhouse Gases and Radiative Forcing

The latest analysis of observations for 2014 from the WMO Global Atmosphere Watch (GAW) Programme shows that the globally averaged mole fractions of carbon dioxide (CO<sub>2</sub>), methane (CH<sub>4</sub>) and nitrous oxide (N<sub>2</sub>O) reached new highs in 2014 (**Figure 12**). Note that there is a one-year lag in the comprehensive reporting of GHG concentrations. The globally averaged CO<sub>2</sub> mole fraction in 2014 reached 397.7±0.1 ppm<sup>3</sup>, 143% of the pre-industrial level. The annual increase from 2013 to 2014 was 1.9 ppm, which is close to the average annual increase within last 10 years and higher than the average growth rate for the 1990s (~1.5 ppm/yr). Preliminary data from NOAA indicate that CO<sub>2</sub> growth has continued at a similar rate in 2015.

The increase in atmospheric CO<sub>2</sub> from 2003 to 2013 corresponds to around 45% of the CO<sub>2</sub> emitted by human activity with the remainder removed by the oceans and the terrestrial biosphere. The smaller growth rate in 2014 in comparison with the previous years is most likely related to the larger annual uptake of CO<sub>2</sub> by the terrestrial biosphere in tropical and subtropical regions.

---

<sup>3</sup> ppm, parts per million. ppb, parts per billion.

Atmospheric CH<sub>4</sub> reached a new high of 1833±1 ppb in 2014, which constitutes 254% of the pre-industrial level, due to increased emissions from anthropogenic sources. Globally averaged CH<sub>4</sub> mole fraction increased by ~9 ppb with respect to 2013. The growth rate of CH<sub>4</sub> decreased from ~13 ppb/yr during the early 1980s to near zero during 1999–2006. However since 2007, atmospheric CH<sub>4</sub> has been increasing again due to increased emissions in tropical and mid-latitude Northern Hemisphere. The average global N<sub>2</sub>O mole fraction in 2014 reached 327.1±0.1 ppb, which is 1.1 ppb above 2013 and 121% of the pre-industrial level (270 ppb). The annual increase from 2013 to 2014 is greater than the mean growth rate over the past 10 years (0.87 ppb/year).

NOAA's Annual Greenhouse Gas Index shows that from 1990 to 2014, radiative forcing by long-lived greenhouse gases increased by 36% with CO<sub>2</sub> accounting for about 80% of this increase. The increase in total radiative forcing by all long-lived greenhouse gases since pre-industrial time reached +2.94 W m<sup>-2</sup>, with CO<sub>2</sub> contributing about 65% (+1.9 W m<sup>-2</sup>), CH<sub>4</sub> about 17% (+0.5 W m<sup>-2</sup>) and N<sub>2</sub>O about 6% (+0.18 W m<sup>-2</sup>) to this total. The total radiative forcing by all long-lived greenhouse gases in 2014 corresponded to a CO<sub>2</sub>-equivalent mole fraction of 481 ppm.

### Stratospheric Ozone and Ozone-depleting Gases

Following the success of the Montreal Protocol, the use of halons and CFCs has been discontinued. However, due to their long lifetime in the atmosphere these compounds will remain in the atmosphere for many decades. There is still more than enough chlorine and bromine present in the atmosphere to cause complete destruction of ozone at certain altitudes in Antarctica from August to December, so the size of the ozone hole from one year to the next is mostly governed by the meteorological conditions.

In 2015, temperatures in the stratosphere have been colder than the long-term average (1979-2014) during the austral winter and spring. The southern polar vortex has been particularly stable and concentric around the South Pole. The area encircled by the vortex has been larger than usual and the average for October was the largest on record. Consequently, the onset of ozone depletion was delayed.

However, once ozone depletion started in mid-August, it proceeded rapidly and the ozone hole area reached a maximum for the season with 28.2 million km<sup>2</sup> on 2<sup>nd</sup> October according to an analysis from the National Aeronautics and Space Administration (NASA, **Figure 13**). Analysis carried out at the Royal Netherlands Meteorological Institute (KNMI) shows that the 2015 ozone hole area reached a maximum of 27.1 million km<sup>2</sup> on 9<sup>th</sup> October. Thus the ozone hole was either the fourth or fifth largest on record after 2000, 2003 and 2006 in both analyses and 1998 in the KNMI analysis.

Taking the 60 consecutive days with the largest areas results in an average ozone hole area of 25.6 million km<sup>2</sup> in 2015, again based on data from NASA. In the KNMI analysis the equivalent area was 24.2 million km<sup>2</sup>, which places the 2015 ozone as the joint second largest (with 1998) behind 2006.

## Tables

**Table 1:** Global average temperature anomaly for 2015 (year to date) and the anomaly for the next warmest year for a range of data sets. Anomalies are expressed relative to 1961-1990 for surface data sets and relative to 1981-2010 for reanalyses.

Data set	Latest month	Anomaly 2015	Next warmest year	Anomaly of next warmest year	Difference
HadCRUT.4.4.0.0	Oct	0.71 ± 0.09	2014	0.57	0.15
NOAAGlobalTemp	Oct	0.74 ± 0.11	2014	0.62	0.11
GISTEMP	Oct	0.72 ± 0.10	2014	0.64	0.08
<b>Combined</b>	<b>Oct</b>	<b>0.73</b>	<b>2014</b>	<b>0.61</b>	<b>0.12</b>
Cowtan and Way	Sep	0.69	2010	0.63	0.06
Berkeley Earth	Sep	0.66	2014	0.59	0.06
<b>Reanalyses</b>					
ERA-Interim	Oct	0.41	2005	0.36	0.04
JRA-55	Oct	0.39	2014	0.30	0.09

**Table 2:** Global average temperature anomaly for 2015 (year to date) and the anomaly for the next warmest year to the same date for a range of data sets. Anomalies are expressed relative to 1961-1990 for surface data sets and relative to 1981-2010 for reanalyses.

Data set	Latest month	Anomaly 2015	Next warmest year-to-date	Anomaly of next warmest year-to-date	Difference
HadCRUT.4.4.0.0	Oct	0.71 ± 0.09	2010	0.58	0.14
NOAAGlobalTemp	Oct	0.74 ± 0.11	2014	0.62	0.13
GISTEMP	Oct	0.72 ± 0.10	2014	0.64	0.08
<b>Combined</b>	<b>Oct</b>	<b>0.73</b>	<b>2010</b>	<b>0.61</b>	<b>0.12</b>
Cowtan and Way	Sep	0.69	2010	0.65	0.04
Berkeley Earth	Sep	0.66	2010	0.61	0.05
<b>Reanalyses</b>					
ERA-Interim	Oct	0.41	2005	0.35	0.05
JRA-55	Oct	0.39	2010	0.31	0.08

## Figures



### Global average temperature anomaly (1850 - October 2015)

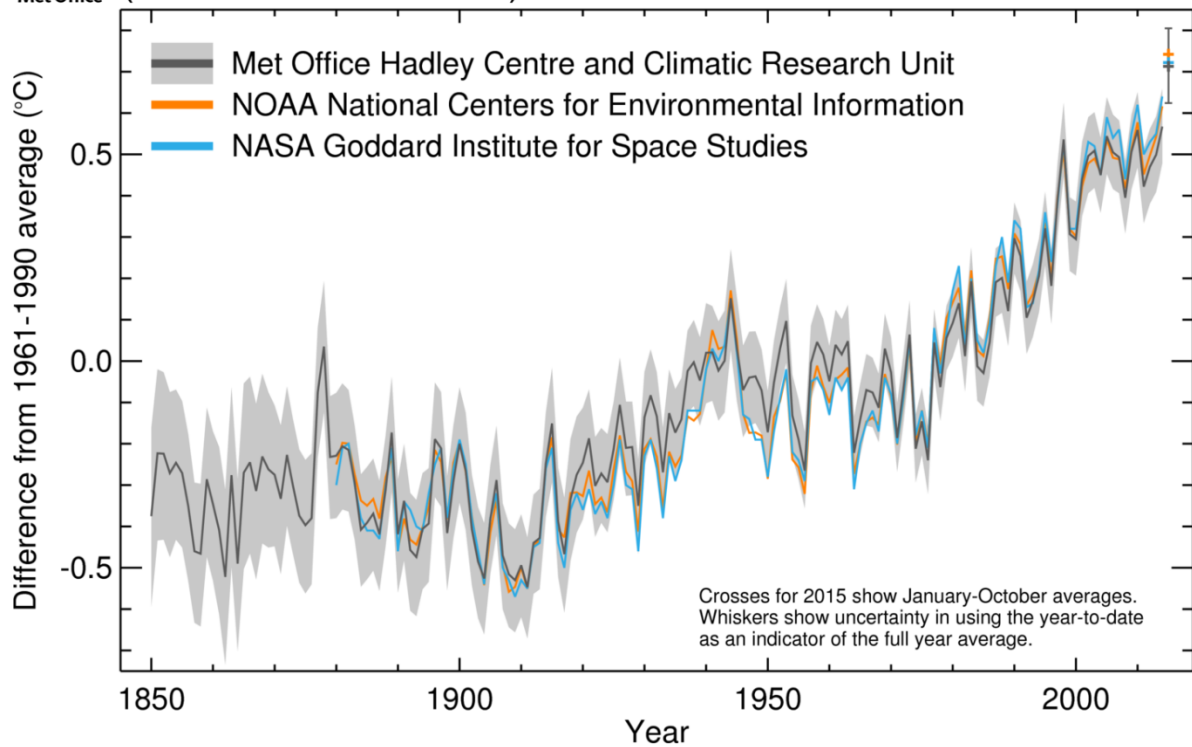


**Figure 1:** Global annual average near-surface temperature anomalies from HadCRUT4.4.0.0 (Black line and grey area indicating the 95% uncertainty range), GISTEMP (blue) and NOAA GlobalTemp (orange). The average for 2015 is a provisional figure based on the months January to October 2015. Source: Met Office Hadley Centre.



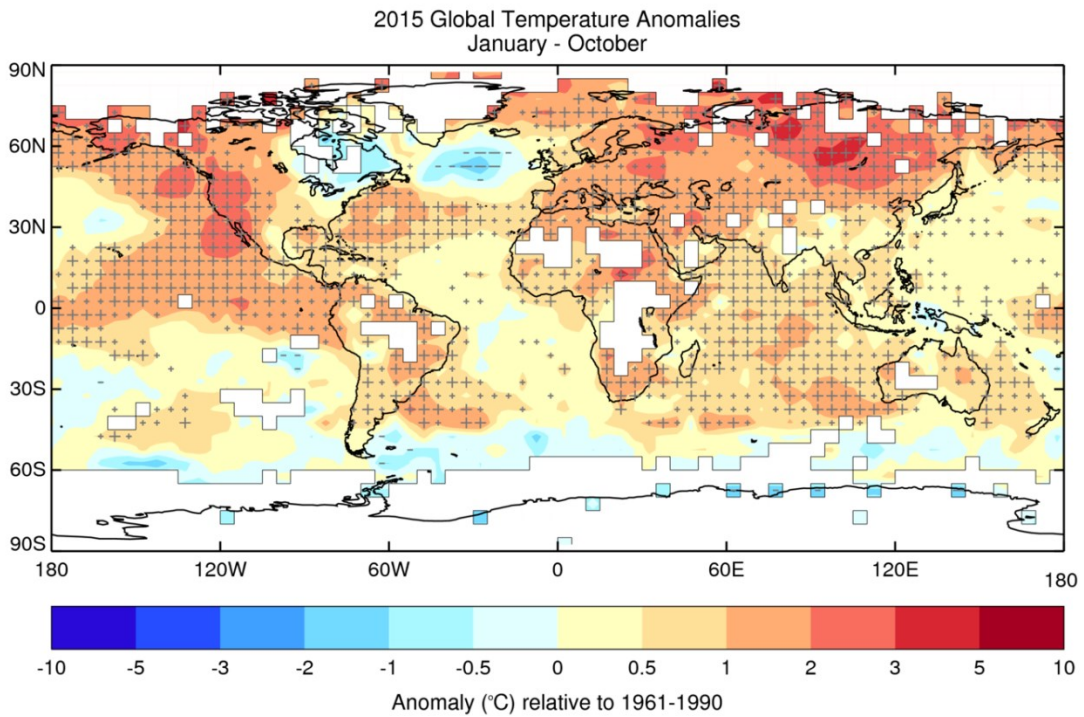


**Figure 2:** Average temperature anomalies for January to October 2014 from the HadCRUT.4.4.0.0 data set. Crosses (+) indicate temperatures that exceed the 90<sup>th</sup> percentile, signifying unusual warmth, and dashes (-) indicate temperatures below the 10<sup>th</sup> percentile, indicating unusually cold conditions. Large crosses and large dashes indicate temperatures outside the range of the 2<sup>nd</sup> to 98<sup>th</sup> percentiles. Source: Met Office Hadley Centre.

Precipitation Percentile GPCC  
January 2015 - October 2015  
(reference period 1951-2010)

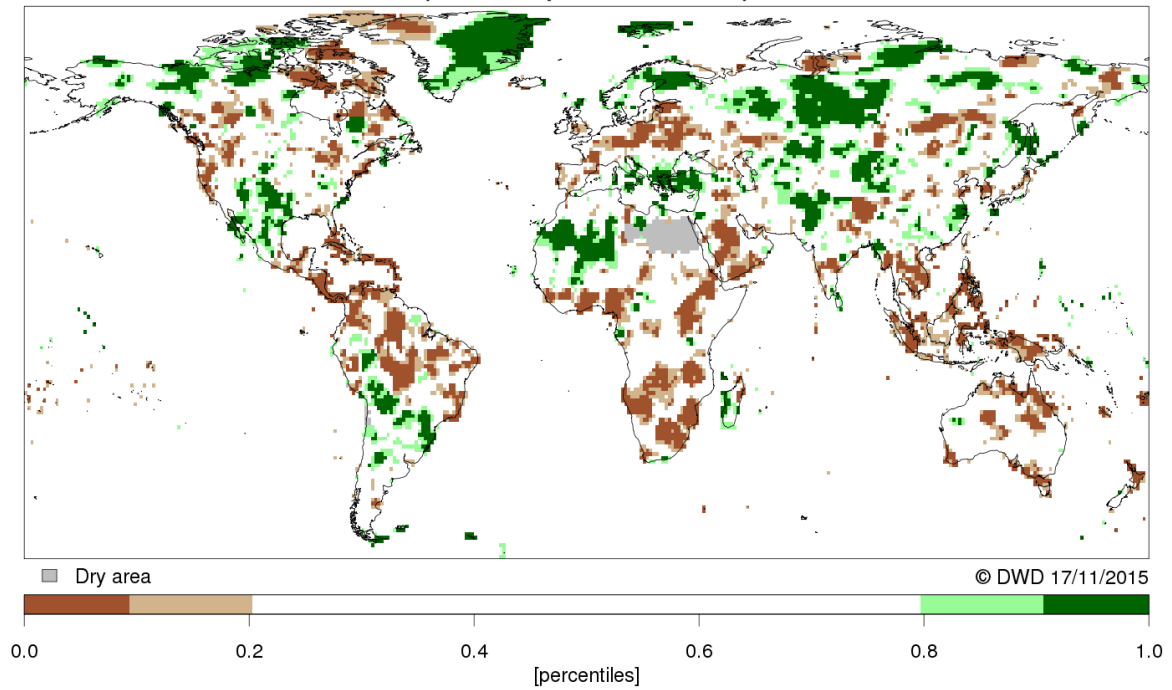


**Figure 3:** 10-month total precipitation anomalies January 2015-October 2015 expressed as percentiles of the 1951-2010 distribution. Source: Global Precipitation Climatology Centre, GPCC, DWD

## SST Anomaly in Niño 3.4 Region (5N-5S,120-170W)

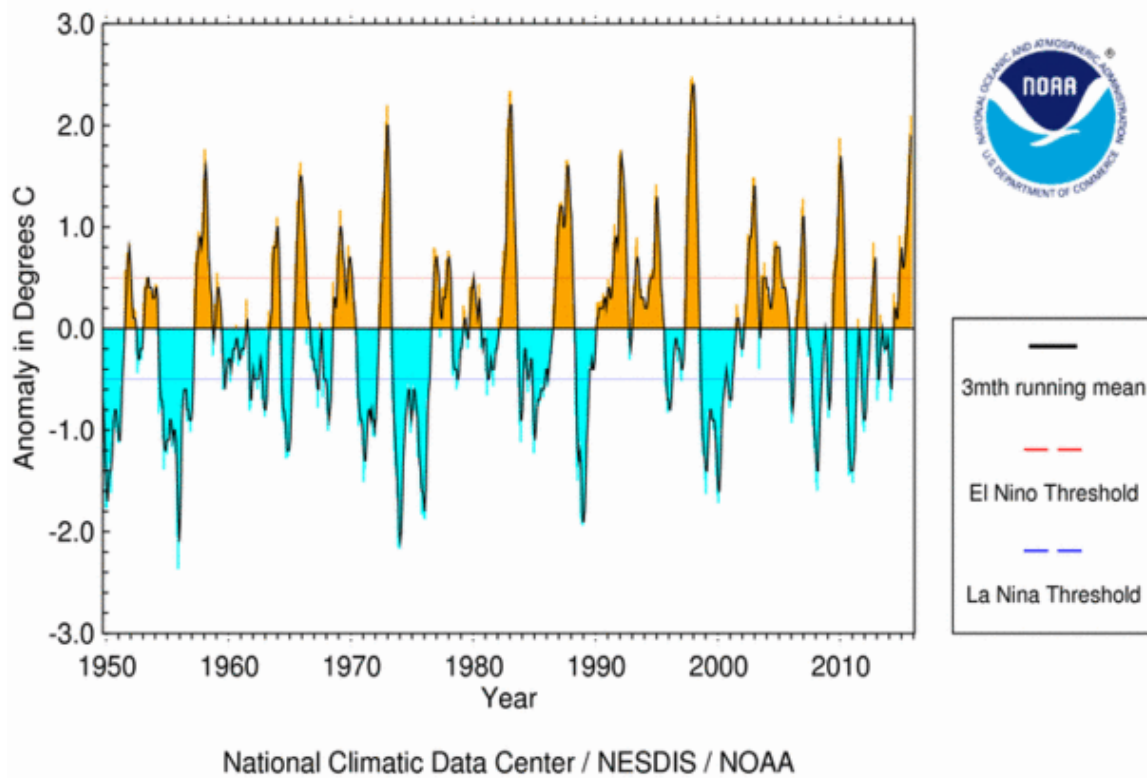


**Figure 4:** Sea-surface temperature anomalies averaged across the Niño 3.4 region. The shaded areas are the monthly anomalies and the solid black line shows the 3-month running mean. Notional El Niño and La Niña thresholds are marked with dotted red and blue lines respectively. Source: NOAA NCEI.

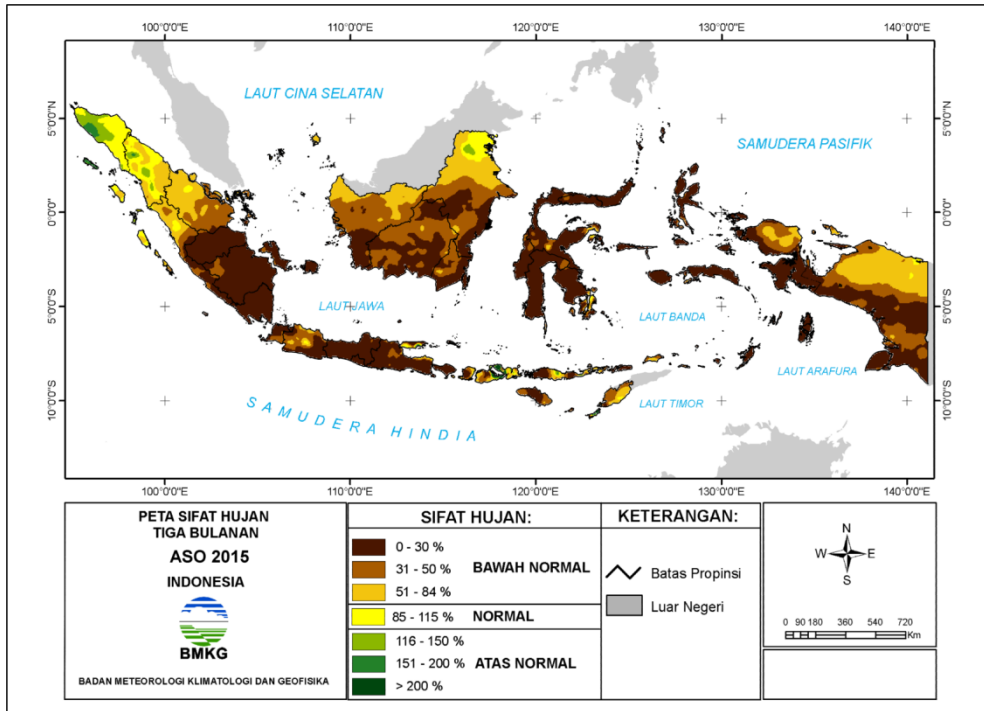


**Figure 5:** *Precipitation percentiles for the three-month period August to October 2015. Large areas of Indonesia were much drier than normal. Source: BMKG.*

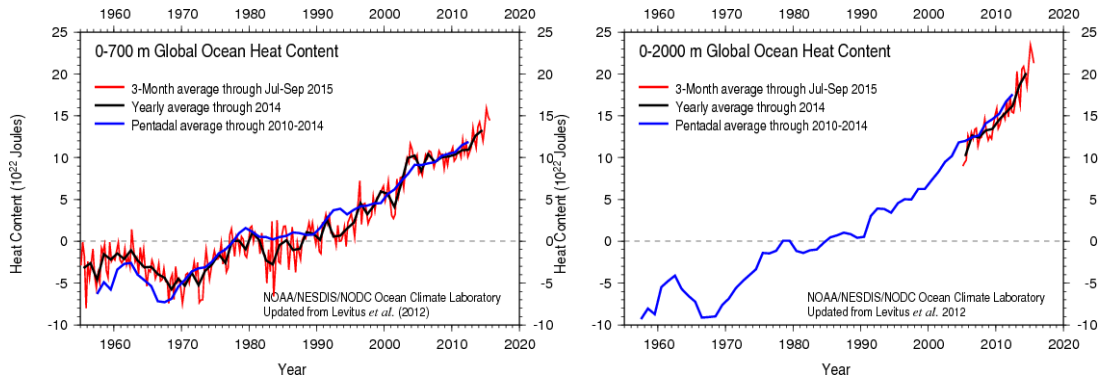


Figure 6: Ocean heat content down to a depth of 700m (left) and 2000m (right). Three-month (red), annual (black) and 5-year (blue) averages are shown. Source: NOAA NCEI.

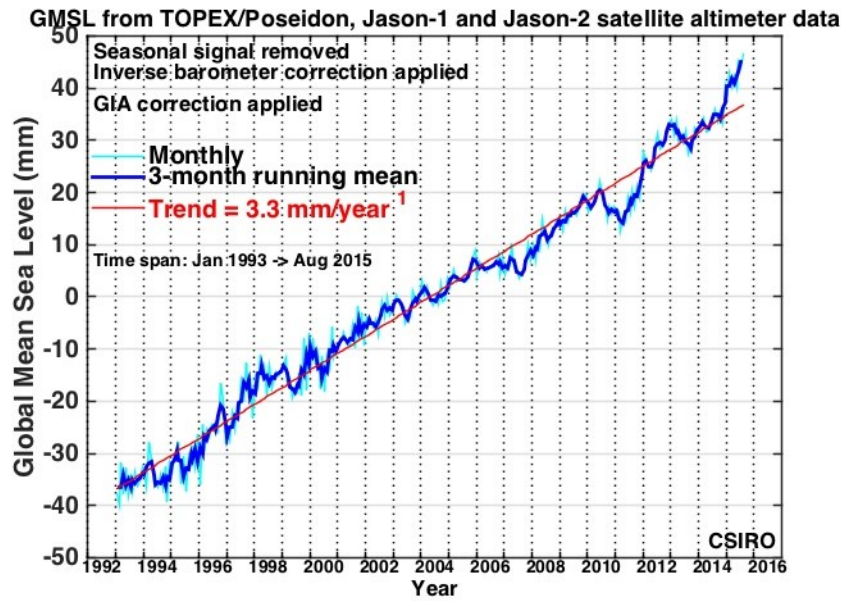
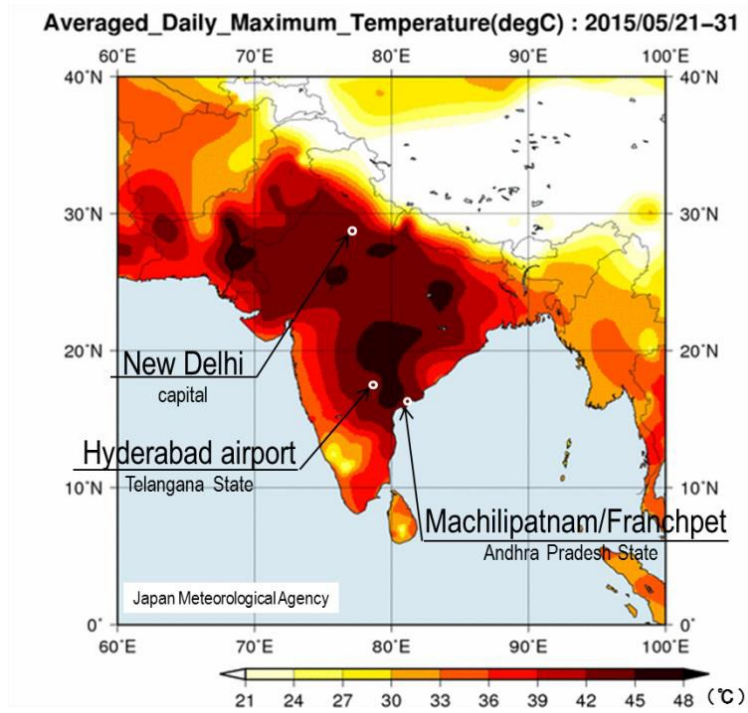


Figure 7: Global average sea level anomalies as estimated from satellite altimeters. The pale blue line shows the monthly average. The dark blue line is the 3-month running mean. The linear trend fit to the data is shown in red. Source: CSIRO.



**Figure 8:** Daily maximum temperature averaged for the period from 21 to 31 May 2015. Source: Tokyo Climate Centre, Japan Meteorological Agency.



**Temperature Anomaly Summer 2015  
(reference period 1961–1990)**

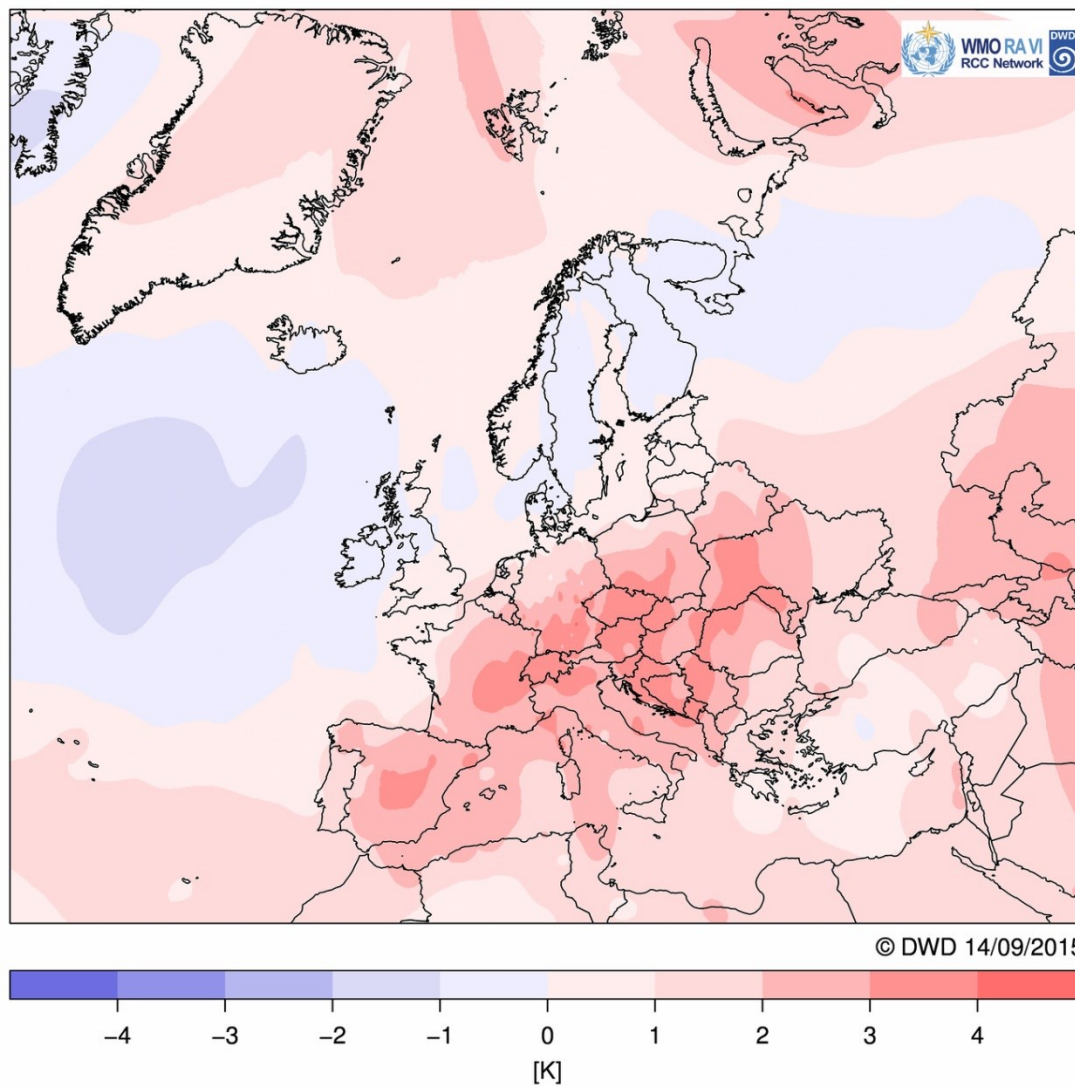


**Figure 9:** European temperature anomalies relative to the 1961-1990 reference period for Summer 2015. Source: DWD

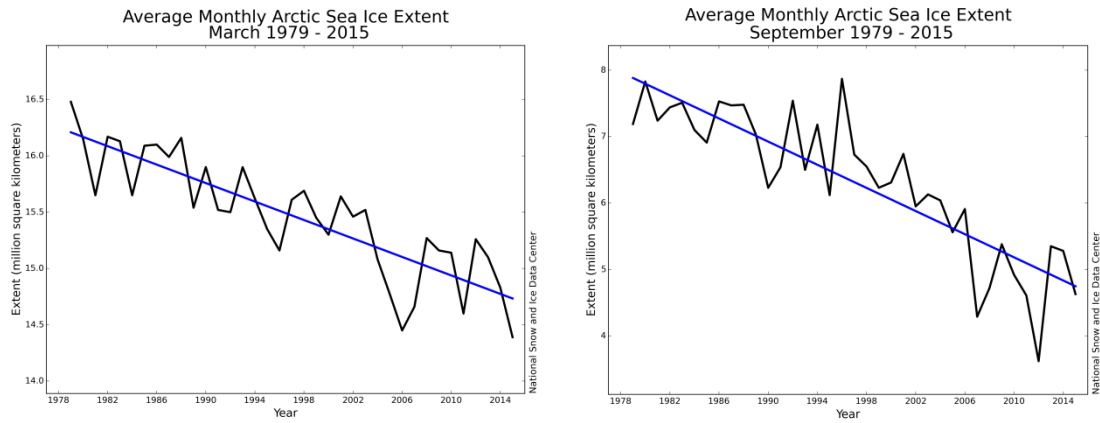


**Figure 10:** Monthly Arctic sea ice extent (in millions of square kilometres) for the modern satellite era (1979-2015) for March (left) and September (right). Images from the National Snow and Ice Data Centre (NSIDC)

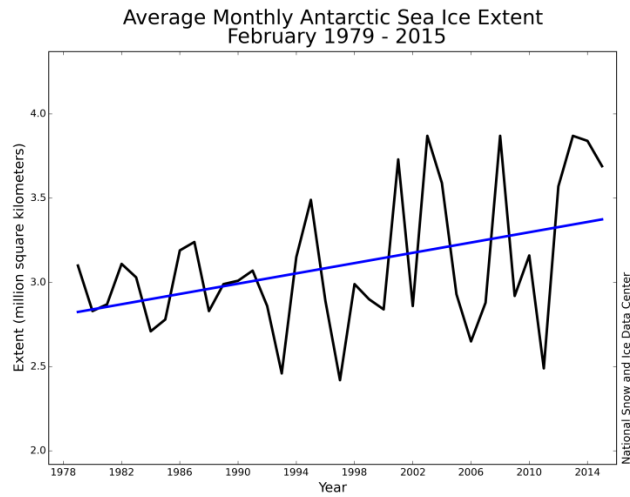


**Figure 11:** Monthly Antarctic sea ice extent (in millions of square kilometres) for the modern satellite era (1979-2015) for February. Image from the National Snow and Ice Data Centre (NSIDC).

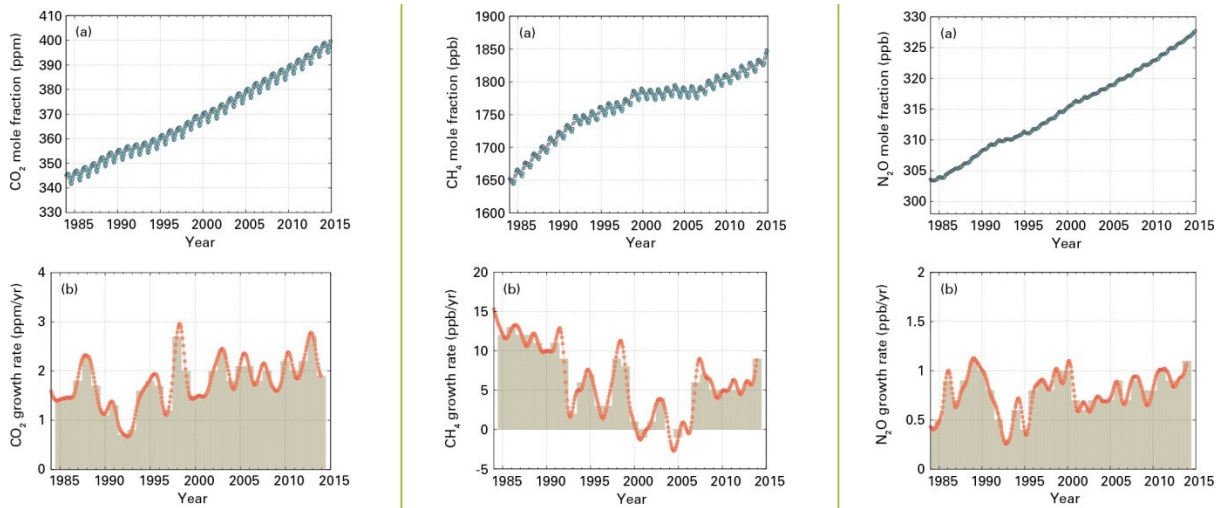


**Figure 12:** (top row) concentrations of averaged concentrations of (left)  $\text{CO}_2$  in parts per million, (middle)  $\text{CH}_4$  in parts per billion and (right)  $\text{N}_2\text{O}$  again in parts per billion from 1984 to 2014. (bottom row) rate of change of concentration.

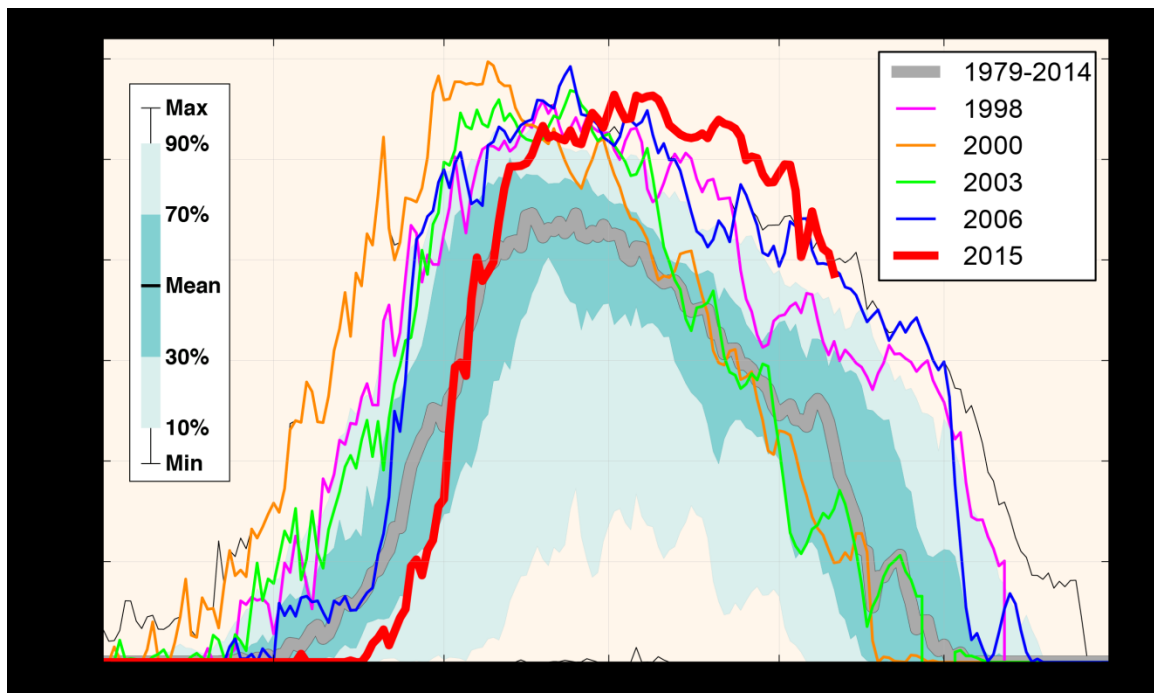


**Figure 13:** Area (millions of  $\text{km}^2$ ) where the total ozone column is less than 220 Dobson units. 2015 is shown in red (until 11 November). Other years characterised by large ozone holes are shown for comparison as indicated by the legend. The smooth, thick grey line is the 1979-2014 average. The dark green-blue shaded area represents the 30th to 70th percentiles and the light green-blue shaded area represents the 10th and 90th percentiles for the time period 1979-2014. The thin black lines show the maximum and minimum values for each day during the 1979-2014 time period. The plot is made at WMO based on data downloaded from the Ozonewatch web site at NASA. The NASA data are based on satellite observations from the OMI and TOMS instruments.

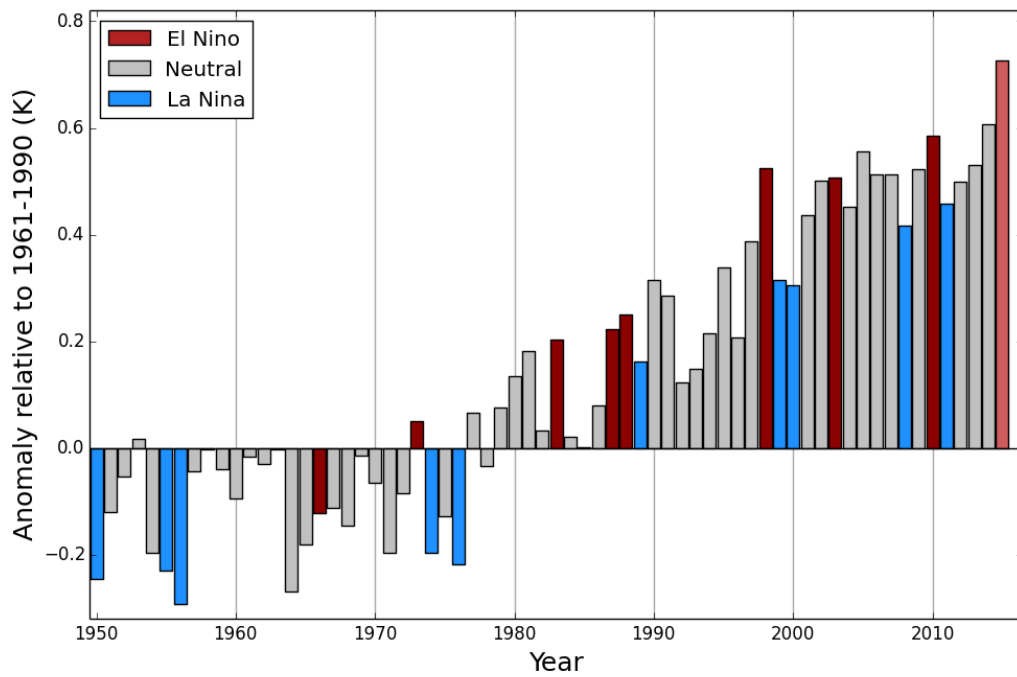


**Figure 14:** global annual average temperatures anomalies (relative to 1961-1990) based on an average of three global temperature data sets (HadCRUT.4.4.0.0, GISTEMP and NOAA GlobalTemp) from 1950 to 2014. The 2015 average is based on data from January to October. Bars are coloured according to whether the year was classified as an El Niño year (red), a La Niña year (blue) or an ENSO-neutral year (grey). Note uncertainty ranges are not shown, but are around 0.1°C.